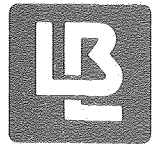


c.2



Lawrence Berkeley Laboratory

UNIVERSITY OF CALIFORNIA

Materials & Molecular Research Division

To be presented at the Third Symposium on Turbulent
Shear Flow, University of California, Davis,
Davis, CA, September 9-11, 1981

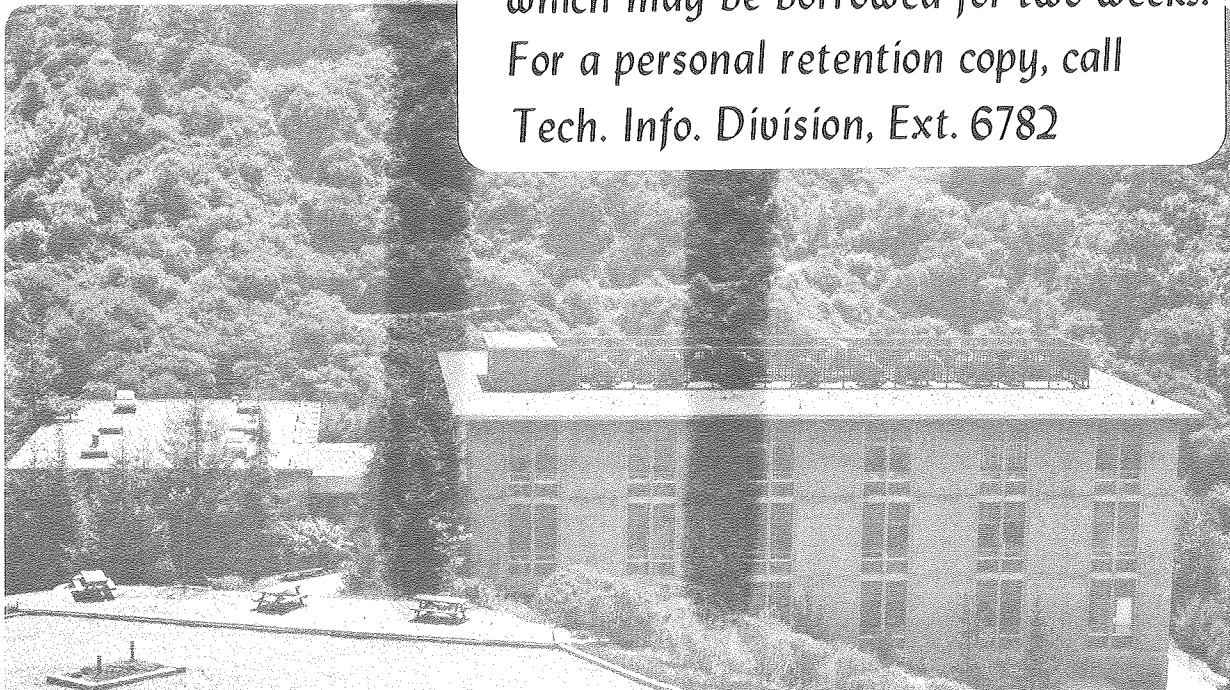
A GENERALIZED ALGEBRAIC RELATION FOR PREDICTING
DEVELOPING CURVED CHANNEL FLOW WITH A $k-\epsilon$ MODEL
OF TURBULENCE

Joseph A.C. Humphrey and Farzad Pourahmadi

June 1981

TWO-WEEK LOAN COPY

*This is a Library Circulating Copy
which may be borrowed for two weeks.
For a personal retention copy, call
Tech. Info. Division, Ext. 6782*



LBL-12009 Rev.
c.2

DISCLAIMER

This document was prepared as an account of work sponsored by the United States Government. While this document is believed to contain correct information, neither the United States Government nor any agency thereof, nor the Regents of the University of California, nor any of their employees, makes any warranty, express or implied, or assumes any legal responsibility for the accuracy, completeness, or usefulness of any information, apparatus, product, or process disclosed, or represents that its use would not infringe privately owned rights. Reference herein to any specific commercial product, process, or service by its trade name, trademark, manufacturer, or otherwise, does not necessarily constitute or imply its endorsement, recommendation, or favoring by the United States Government or any agency thereof, or the Regents of the University of California. The views and opinions of authors expressed herein do not necessarily state or reflect those of the United States Government or any agency thereof or the Regents of the University of California.

by

Joseph A.C. Humphrey and Farzad Pourahmadi

Lawrence Berkeley Laboratory
Department of Mechanical Engineering
University of California
Berkeley, California 94720

ABSTRACT

Using algebraic approximations for the Reynolds stress equations a general expression has been derived for C_μ in $v_t = C_\mu k^2/\epsilon$ which accounts simultaneously for the effects of streamline curvature and pressure-strain in the flow, including wall-induced influences on the velocity fluctuations. The expression derived can be shown to encompass similar but more specific formulations proposed by Bradshaw, Rodi, and Leschziner and Rodi. The present formulation has been used in conjunction with a k - ϵ model of turbulence to predict developing, two-dimensional, curved channel flows where both curvature and pressure-strain effects can be large. Minor modifications to include the influence of curvature on the length scale of the flow near the walls produce a significant improvement in the calculations. While, in general, predictions are in good agreement with experimental measurements of mildly and strongly curved flows, the model tends to overpredict the kinetic energy of turbulence in the inner-radius (convex) wall region. This is attributed to a breakdown of the assumption that $\overline{u_i u_j}/k$ is a constant in the derivation of the general expression for C_μ . Most of the experimental results suggest the presence of a weak cross-stream motion due to Taylor-Görtler vortices which cannot be resolved by the calculation scheme. Despite its limitations the present formulation provides a degree of generality not previously available in two-equation modeling of turbulent flows.

INTRODUCTION

The importance of experimental measurements and theoretical predictions of turbulent flows over convex and concave surfaces and in curved channels is evidenced by the attention which these two topics have and continue to receive in relation to, for example, flow cooling and erosion of turbine blades and rocket nozzles, flows in compressors, turbomachinery, curved diffusers and channel passages. Cases of studies pertaining to flows over convex surfaces are given in [1-7] while similar examples pertaining to flows over concave surfaces are available in [4-7]. Curved channel studies, where both a convex and a concave surface influence the flow, have been reported in [7-16].

In an extensive review of the subject Bradshaw [17] evidences the sensitivity of turbulent flow characteristics to even small amounts of mean streamline curvature. Thus, for example, in the early study by Kreith [18] and in subsequent investigations by Thomann [19] and Mayle et al. [20] it has been shown that the heat flux through the concave wall of a

curved channel can be up to 33 percent larger, and through the convex wall 15 percent smaller, relative to that through the walls of a straight channel. A similar experimental heat transfer study by Brinich and Graham [13] (not entirely free of side-wall-driven secondary motion) confirms this result and, in addition, shows that while friction on the inner curved wall of a channel can fall below the values for a straight channel, friction measurements on the outer curved wall yield increases of about 50 percent.

Three-Dimensional Motions in Curved Channel Flows

Hunt and Joubert [14] make a distinction between two types of curved channel flows: a) 'shear-dominated' flows with small curvature effects, ($R_c/D > 20$, approximately), and b) 'inertia-dominated' flows with large curvature effects ($R_c/D < 20$, approximately). In their study the channel mean radius of curvature R_c was large relative to the channel width D , ($R_c/D = 100$). Thus, the flow investigated was a 'curvature-perturbed straight flow' as opposed to a flow strongly influenced by stream-line curvature. Measurements at three Reynolds numbers ($Re = DU_m/\nu$; U_m = maximum velocity and ν = kinematic viscosity) corresponding to $3 \cdot 10^4$, $6 \cdot 10^4$ and $1.3 \cdot 10^5$ respectively, indicated small variations of about 2% in the longitudinal mean velocity component. Detailed characterization of this velocity component for $Re = 6 \cdot 10^4$ revealed a Taylor-Görtler vortex pattern [21-23] in the central flow region. The authors comment that the end-wall vortices in the curved channel "appear to fix the position of the central region structure" although earlier studies [11,24] cite an independence of end wall conditions. The cellular structure found by Hunt and Joubert has been observed in other curved channel flows, both in laminar [4,25] and turbulent regime [4,9], and in boundary layers developing on concave walls [4,11,23,24]. The onset and subsequent amplification of longitudinal vortices is characterized by the Görtler parameter which is defined by $G_T = 43(\theta/R_o)^{1/2}$; where θ is the boundary layer momentum thickness and R_o the concave wall radius of curvature. Tani [4] shows that for $G_T \leq 0.35$ longitudinal vortices will be damped in turbulent flow, while for values $G_T \geq 0.35$ amplification depends on the value of the vortex spacing parameter $\lambda \theta$ and the curvature parameter λR_c ; where λ is the spacing between vortices. In the study by Hunt and Joubert

$G_T = 0.87$, $\lambda \theta = 0.57$ and $\lambda R_c = 1430$ corresponding, in principle, to a marginally stable flow (which it was not). Using a stability limit proposed by Lezius and Johnston [26] for Taylor-Görtler vortices in rotating duct flow, Hunt and Joubert find that such vortices are amplified in curved channel flows with $R_c/D \lesssim 90$. Again, when applied to their flow, the criterion suggests that it should be marginally stable and free of three-dimensional structure.

Although not reported by the authors there is evidence in the study by Eskinazi and Yeh [8] ($R/D = 9.5$) supporting the contention that their flow contained Taylor-Görtler vortices. As in [14] measurements of shear stress across the channel show good agreement with theoretical prediction in the inner-radius flow region. However, the data for the outer-radius flow region are in disagreement with the distribution expected from the wall shear measurements and, as pointed out in [14], is most likely an indication of the existence of a weak secondary flow.

Finally, it is important to note that Ellis and Joubert [9] specifically remark on having observed Taylor-Görtler effects for a radius ratio $R_c/D = 30$ but not for $R_c/D = 6$. This finding contradicts expectations based on the stability considerations outlined above and suggests that turbulence diffusion and pressure redistribution in the flow near the outer-radius wall of a strongly curved channel may be responsible for 'smearing out' three-dimensional time averaged structures which otherwise would be observed. The net effect of these structures can then be looked upon as contributing to the overall process of enhanced mixing and turbulence activity in the outer-radius wall region of the flow.

The Prediction of Curved Channel Flows

As discussed above, concavely curved flows are prone to three-dimensional instabilities, but for purposes of numerical computation they are commonly presumed to be two-dimensional in their mean structure. Thus, for example, Simon and Honami [27] include the study of Hunt and Joubert [13] among the experimental data sets recommended for the testing of two-dimensional turbulent flow computational procedures dealing with boundary layer flows with streamwise curvature. Concave wall boundary layer development predictions of longitudinal velocity in [7] are based on the two-dimensionality assumption and show good agreement with experimental measurements. However, similar calculations for friction factors [6] and turbulent shear stress [11] seriously underpredict the values of these parameters in the flow region adjacent to the concave wall. Likewise, while the fully developed curved channel longitudinal velocity predictions of [7] are in good agreement with experimental measurements of [9] for $R_c/D = 6$ over most of the channel width, between $(r - r_i)/(r_o - r_i) = 0.85$ and 0.96 velocity is underpredicted by approximately 9%. A similar discrepancy does not arise at the inner radius wall of this flow. One might attribute the above lack of agreement between measurements and calculations to three-dimensional Taylor-Görtler effects as, for example, implied in [11]. However, it also seems reasonable to suspect that the influence of streamline curvature and/or wall effects on turbulent mixing at concave walls may have been underestimated. That, in fact, higher levels of turbulent diffusion should arise than were actually predicted by the models employed.

It is argued in, for example, [2,6] that only turbulence modeling approaches based on the calculation of Reynolds stresses directly from their transport equations can accurately account for streamline curvature and wall pressure effects in curved channel flows. Simpler approaches such as in [7], based on a two-equation ($k-\epsilon$) model of turbulence, require empirical modeling of curvature effects in the equation for dissipation of kinetic energy of turbulence and the definition of a new model constant which must be optimized numerically. Even simpler approaches based on the mixing-length concept, such as in [10], are seriously limited by the need to prescribe different mixing-length variations for differently curved flows.

The present work shows that the $k-\epsilon$ model of turbulence can be extended to predict developing curved channel flows if C_μ in the expression for turbulent viscosity (μ_t):

$$\mu_t/\rho = C_\mu \underbrace{(k^{3/2}/\epsilon)}_{\ell_o} \underbrace{k^{1/2}}_{v_o} \quad (1)$$

is made an appropriate function of streamline curvature and accounts for pressure-strain and wall-induced effects. In Eq. (1) ρ is density, k is the kinetic energy of turbulence and ϵ is the rate of dissipation of k . The symbols ℓ_o and v_o denote characteristic length and velocity scales of turbulence respectively, determined from transport equations for k and ϵ . The essence of the approach pursued in this study is then, that the product $C_\mu \ell_o$ in Eq. (1) should yield a modified length scale of turbulence (ℓ) which reflects the direct influence of streamline curvature and pressure-strain in the flow. Calling $C_{\mu o}$ the value of C_μ in the absence of these effects it is clear that:

$$\ell = (C_\mu/C_{\mu o}) \ell_o \quad (2)$$

If the local-equilibrium approximation is made it can be shown [28] that $C_{\mu o} \approx 0.12$. The recommended experimental value is $C_{\mu o} = 0.09$.

It has been argued by Wilcox and Chambers [1] and by So [15] that it is not ℓ_o but v_o in Eq. (1) which should be modified for the influence of curvature effects. Their arguments are based on the observation that the transport equation for k does not manifest an explicit dependence on Coriolis and centrifugal accelerations and that, as a consequence, $v_o \equiv k^{1/2}$ misrepresents the turbulence velocity scale. The study by So [15], for example, is based entirely on the assumption that the turbulence length scale is unaffected by streamline curvature. However, there is ample experimental evidence in the work by Eskinazi and Yeh [8] showing that both the microscale and the integral scale of turbulence are increased at the concave wall and decreased at the convex wall of curved channel flow. More recently, Prabhu and Sundarasiva Rao [16] have shown that the mean inclination of large scale structures in curved channel flow also depends strongly on curvature. The essence of their finding is that large eddies are 'flattened' more near the convex wall of a curved channel than in the concave wall region.

For models based on the notion of a turbulent viscosity as defined by Eq. (1) it would seem to be immaterial which of the two scales (ℓ_o or v_o) is modi-

fied to include the influence of curvature (and related effects). However, because it will be consistent with subsequent modifications to be made to the turbulence model, it will be the length scale which is modified in this work. This approach is consistent with that proposed by Bradshaw [17] on heuristic grounds for mildly curved flows and parallels to some extent various ideas set forth in the studies of Gibson [2], Irwin and Arnot Smith [6], So [15], Ljuboja and Rodi [29] and Leschziner and Rodi [30]*. The general expression derived here for C_μ includes as subsets the more specific expressions derived in [28-30] and yields as a special limiting case Bradshaw's proposal [17]:

$$\ell = \left(1 \pm \beta \frac{U_\theta/r}{\partial U_\theta/\partial r}\right) \ell_0 \quad (3)$$

for the turbulence length scale in mildly curved channel flows. In Eq. (3) β is an empirical constant of order 10, r is the radial coordinate direction (transverse to the flow) and U_θ is the value of the local longitudinal (streamwise) component of mean velocity along a streamline of curvature radius r .

The modified form of the k - ϵ model derived here, with a general formulation for C_μ , offers a compromise between the potentially more accurate but more costly Reynolds stress model closures and the simpler but considerably more restrictive mixing-length calculation approaches. In this study attention is fixed principally on flows in channels with relatively strong curvature ($R_c/D \leq 20$) in which inertial effects are dominant. Nevertheless, as will be shown, the extended form of the model has also been applied successfully to channel flows with mild curvature.

GOVERNING EQUATIONS AND BOUNDARY CONDITIONS

The continuity and momentum equations governing steady, two-dimensional, turbulent, incompressible, developing curved channel flows are:

Continuity

$$\frac{\partial U_r}{\partial r} + \frac{1}{r} \frac{\partial U_\theta}{\partial \theta} + \frac{U_r}{r} = 0 \quad (4)$$

r-Momentum

$$\rho \left[U_r \frac{\partial U_r}{\partial r} + \frac{U_\theta}{r} \frac{\partial U_r}{\partial \theta} - \frac{U_\theta^2}{r} \right] = -\frac{\partial P}{\partial r} + \frac{1}{r} \frac{\partial}{\partial r} (\mu_{eff} r \frac{\partial U_r}{\partial r}) + \frac{1}{r} \frac{\partial}{\partial \theta} (\mu_{eff} \frac{1}{r} \frac{\partial U_r}{\partial \theta}) - \mu_{eff} \frac{U_r}{r^2} - \mu_{eff} \frac{2}{r^2} \frac{\partial U_\theta}{\partial \theta} + S_r \quad (5)$$

θ -Momentum

$$\rho \left[U_r \frac{\partial U_\theta}{\partial r} + \frac{U_\theta}{r} \frac{\partial U_\theta}{\partial \theta} + \frac{U_r U_\theta}{r} \right] = -\frac{1}{r} \frac{\partial P}{\partial \theta} + \frac{1}{r} \frac{\partial}{\partial r} (\mu_{eff} r \frac{\partial U_\theta}{\partial r}) + \frac{1}{r} \frac{\partial}{\partial \theta} (\mu_{eff} \frac{\partial U_\theta}{\partial \theta}) - \mu_{eff} \frac{U_\theta}{r^2} + \mu_{eff} \frac{2}{r^2} \frac{\partial U_r}{\partial \theta} + S_\theta \quad (6)$$

* Reference [30] came to our attention after the present study was completed.

In the above equations the Reynolds stresses have been modeled according to the Boussinesq assumption which relates turbulent stresses to velocity gradients through a turbulent viscosity. The effective viscosity μ_{eff} is the sum of the laminar flow viscosity (μ) and the turbulent viscosity (μ_t), with the latter given by Eq. (1). The terms S_r and S_θ in equations (5) and (6) are given by:

$$S_r = \frac{1}{r} \frac{\partial}{\partial \theta} (\mu_t r \frac{\partial}{\partial r} (\frac{U_\theta}{r})) + \frac{1}{r} \frac{\partial}{\partial r} (\mu_t r \frac{\partial U_r}{\partial r}) - \mu_t \frac{U_r}{r^2} \quad (7)$$

$$S_\theta = \frac{1}{r} \frac{\partial}{\partial \theta} (\mu_t (2 \frac{U_r}{r} + \frac{1}{r} \frac{\partial U_\theta}{\partial \theta})) + \frac{\partial}{\partial r} (\frac{\mu_t}{r} (\frac{\partial U_r}{\partial \theta} - U_\theta)) + \frac{\mu_t}{r} (\frac{\partial U_\theta}{\partial r} - \frac{U_\theta}{r}) \quad (8)$$

In order to solve for the spatial variation of μ_t transport equations are required for k and ϵ . Following the modeling approach outlined in [31] (based on the earlier work of [32,33]) but restricted here to two-dimensional cylindrical coordinates yields:

Kinetic energy of turbulence, (k)

$$\rho \left[U_r \frac{\partial k}{\partial r} + \frac{U_\theta}{r} \frac{\partial k}{\partial \theta} \right] = \frac{1}{r} \frac{\partial}{\partial r} (\frac{\mu_{eff}}{\sigma_k} r \frac{\partial k}{\partial r}) + \frac{1}{r^2} \frac{\partial}{\partial \theta} (\frac{\mu_{eff}}{\sigma_k} \frac{\partial k}{\partial \theta}) + P - \rho \epsilon \quad (9)$$

Dissipation of kinetic energy of turbulence, (ϵ)

$$\rho \left[U_r \frac{\partial \epsilon}{\partial r} + \frac{U_\theta}{r} \frac{\partial \epsilon}{\partial \theta} \right] = \frac{1}{r} \frac{\partial}{\partial r} (\frac{\mu_{eff}}{\sigma_\epsilon} r \frac{\partial \epsilon}{\partial r}) + \frac{1}{r^2} \frac{\partial}{\partial \theta} (\frac{\mu_{eff}}{\sigma_\epsilon} \frac{\partial \epsilon}{\partial \theta}) + C_{\epsilon 1} \frac{\epsilon}{k} P - C_{\epsilon 2} \rho \frac{\epsilon^2}{k} \quad (10)$$

with the production term "P" given by:

$$P = \mu_t \left\{ 2 \left[\left(\frac{\partial U_r}{\partial r} \right)^2 + \left(\frac{1}{r} \frac{\partial U_\theta}{\partial \theta} \right)^2 - \frac{U_\theta}{r} \left(\frac{1}{r} \frac{\partial U_r}{\partial \theta} + \frac{\partial U_\theta}{\partial r} \right) + \frac{U_r}{r} \left(\frac{U_r}{r} + \frac{2}{r} \frac{\partial U_\theta}{\partial \theta} \right) + \frac{1}{r} \frac{\partial U_r}{\partial \theta} \frac{\partial U_\theta}{\partial r} \right] + \left(\frac{U_\theta}{r} \right)^2 + \left(\frac{\partial U_\theta}{\partial r} \right)^2 + \left(\frac{1}{r} \frac{\partial U_r}{\partial \theta} \right)^2 \right\} \quad (11)$$

Values of the constants in the above equations were set in accordance with the recommendations of [33]:

$C_{\epsilon 1} = 1.44$, $C_{\epsilon 2} = 1.92$ and $\sigma_k = 1.0$. However, the value of σ_ϵ (customarily fixed to 1.3) was allowed to vary with radial location as described further below.

In order to solve Eqs. (4-6, 9 and 10) boundary conditions for U_θ , U_r , k and ϵ are necessary and are summarized in Table 1. The table indicates that velocity components were set equal to zero at the wall. However, in order to economize on calculations the region between a curved wall and the node P closest to that wall was bridged by the standard logarithmic velocity profile:

$$\frac{[U_\theta]_P}{[\tau_w/\rho]^{1/2}} = A \ln \left[\frac{y_P (\tau_w/\rho)^{1/2}}{\nu} \right] + B \quad (12)$$

where subscript P denotes the grid node position nearest to the wall, y is the distance from the wall and τ_w is the wall shear stress. Values of the law of the wall constants were set to $A = 2.39$ and $B = 5.45$. Assuming local-equilibrium of the flow in near-wall regions, the law of the wall relation yields:

$$\tau_w \approx \tau_P = \frac{\rho C_{\mu 0}^{1/4} k_P^{1/2} [U_\theta]_P}{A \ln \left[\frac{y_P C_{\mu 0}^{1/4} k_P^{1/2}}{\nu} \right] + B} \quad (13)$$

It is the value of τ_w which is actually used as the wall boundary condition in the calculation scheme. It should be mentioned that an attempt was made to reflect the presence of curvature effects in the law of the wall by using an equivalent form of Eq. (8) in the paper by Meroney and Bradshaw [11]. Since this approach did not yield a significant improvement in the calculations the simpler logarithmic relation given by Eq. (12) above was adhered to.

	Inlet Plane	Exit Plane	At Curved Walls
U_θ	Prescribed from Experiment	Prescribed from Experiment	τ_w specified through Eq. (13)
U_r	0	$\frac{\partial U_r}{\partial \theta} = 0$	τ_w specified through Eq. (13)
k	$0.005(U_\theta^2)_{\text{inlet}}$	$\frac{\partial k}{\partial \theta} = 0$	Prescribed from a simplification of the k and ϵ equations at the walls. See discussion in text.
ϵ	$\frac{(k^{3/2})_{\text{inlet}}}{0.01 D}$	$\frac{\partial \epsilon}{\partial \theta} = 0$	

TABLE 1: Boundary Conditions for Curved Channel Flows

The wall value of kinetic energy of turbulence, k_p , was found from its standard transport equation with the flux from the wall set equal to zero and the production term modified to include the wall shear stress as given by Eq. (13). The wall value of dissipation of kinetic energy, ϵ_p , was initially determined by requiring that the turbulence length scale vary linearly with distance from the wall. Thus, substituting the expression for $(\partial U_\theta/\partial y)_P$ from the law of the wall into the simplified (near-wall region) turbulent kinetic energy balance yields:

$$\epsilon_P = \frac{C_{\mu 0}^{3/4} k_P^{3/2}}{\ell_0} \quad (14)$$

Where the turbulence length scale is given by $\ell_0 = \kappa y_P$ and κ is the Von Karman universal constant. Following Bradshaw [17], the extra-stain influence due to curvature effects on the magnitude of the turbulence length scale near the walls can be modeled according to Eq. (3) for regions of the flow in which $\delta \equiv |(U_\theta/r)/(\partial U_\theta/\partial r)| \leq 0.05$. Thus, an expression for

dissipation at the near-wall node P which includes the influence of streamline curvature effects is:

$$\epsilon_P = \frac{C_{\mu 0}^{3/4} k_P^{3/2}}{\kappa' y_P} \quad (15)$$

where $\kappa' = \kappa(1 \pm \beta \delta_P)$.

Following Launder and Spalding [33], the equation for dissipation of kinetic energy in the near wall region simplifies to:

$$0 = \frac{1}{r} \frac{\partial}{\partial r} \left(\frac{\nu_t}{\sigma_\epsilon} r \frac{\partial \epsilon}{\partial r} \right) + C_{\epsilon 1} \frac{\epsilon}{k} P - C_{\epsilon 2} \frac{\epsilon^2}{k} \quad (16)$$

Assuming local-equilibrium in the flow and recalling Eqs. (1) and (15) the above expression may be rewritten:

$$0 = \frac{1}{r} \frac{\partial}{\partial r} \left(\frac{C_{\mu 0} k^2/\epsilon}{\sigma_\epsilon} r \frac{\partial \epsilon}{\partial r} \right) + (C_{\epsilon 1} - C_{\epsilon 2}) C_{\mu 0}^{3/2} \left(\frac{k}{\kappa' y} \right)^2 \quad (17)$$

Further assuming that $\frac{\partial k}{\partial r} = 0$ in the near wall region [33] it may be shown that Eq. (17) simplifies to the following curvature-modified expression for σ_ϵ :

$$\sigma_\epsilon = \frac{\kappa'^2}{(C_{\epsilon 2} - C_{\epsilon 1}) C_{\mu 0}^{1/2}} \quad (18)$$

In the standard form of the k- ϵ model of turbulence the value of σ_ϵ is fixed to the wall value of 1.3 throughout the flow [33]. In this study σ_ϵ at any radial location was linearly interpolated from the near-wall grid node values determined by means of Eq. (18).

GENERAL EXPRESSION FOR C_μ

Prior to outlining the detailed derivation of the general form of the C_μ coefficient, it is instructive to justify by means of a simple example the advantages in an improved modeling of this coefficient. Combination of Eqs. (1-3) readily yields the expression:

$$\mu_t/\rho = C_{\mu 0} \ell_0 (1 \pm \beta \delta) \nu_0 \quad (19)$$

This equation is a limiting form of the more general relation sought in this study. While Eq. (19) accounts for the influence of mild curvature effects on the turbulence length scale ℓ_0 through the curvature parameter $(1 \pm \beta \delta)$ a more general relationship is desirable, in which arbitrary streamline curvature, pressure-strain and wall pressure corrections are simultaneously included. The purpose of this section is to outline the derivation of this more general expression, obtained by substitution of an expression for the turbulent shear stress (determined from an algebraic-stress model) into a Boussinesq approximation for the shear stress in which the turbulent viscosity is given by Eq. (1).

The Reynolds Stress Equations

The starting point for the present analysis is the high-Reynolds number form of the $u_i u_j$ transport equation given in [29]. In three-dimensional Cartesian coordinate notation and neglecting molecular diffusion this equation is:

$$\begin{aligned} u_k \frac{\partial \overline{u_i u_j}}{\partial x_k} = & - \left(\overline{u_j u_k} \frac{\partial U_i'}{\partial x_k} + \overline{u_i u_k} \frac{\partial U_j'}{\partial x_k} \right) - 2\nu \frac{\partial \overline{u_i}}{\partial x_k} \frac{\partial \overline{u_j}}{\partial x_k} \\ & P_{ij} \quad \quad \quad \epsilon_{ij} \quad (20) \\ & + \frac{P}{\rho} \left(\frac{\partial \overline{u_i}}{\partial x_j} + \frac{\partial \overline{u_j}}{\partial x_i} \right) - \frac{\partial}{\partial x_k} \left\{ \overline{u_i u_j u_k} + \frac{P}{\rho} (\delta_{jk} u_i + \delta_{ik} u_j) \right\} \\ & \Pi_{ij} \quad \quad \quad D_{ij} \end{aligned}$$

In the above equation P_{ij} represents the production of $\overline{u_i u_j}$ and requires no approximation. Viscous dissipation (ϵ_{ij}) and contributions to the pressure-strain term (Π_{ij}) were modeled as in [29]. The forms of these terms are:

$$\epsilon_{ij} = \frac{2}{3} \epsilon \delta_{ij} \quad (\text{isotropic dissipation}) \quad (21)$$

and

$$\Pi_{ij} = \Pi_{ij,1} + \Pi_{ij,2} + \Pi'_{ij,1} + \Pi'_{ij,2} \quad (22)$$

In Eq. (22) $\Pi_{ij,1}$ represents contributions to the pressure-strain arising from fluctuating velocities only, while $\Pi_{ij,2}$ accounts for the interaction between the mean strain and fluctuating velocities. The additional contributions $\Pi'_{ij,1}$ and $\Pi'_{ij,2}$ represent pressure-strain corrections due to the effect of walls on the level of turbulent fluctuations in the flow. These terms were modeled as shown in Table 2 and correspond to model 2 of [34]. Values of the model constants are also given in the table.

The diffusive transport of $\overline{u_i u_j}$ is attributed primarily to turbulent velocity fluctuations [34] for which the simple gradient diffusion hypothesis of Daly and Harlow [35] yields:

$$- \overline{u_i u_j u_l} = C'_s \frac{k}{\epsilon} \overline{u_l u_m} \frac{\partial \overline{u_i u_j}}{\partial x_m} \quad (23)$$

where C'_s is an empirically determined constant (not needed in this study).

The "f" Wall Function

In the approximations for $\Pi'_{ij,1}$ and $\Pi'_{ij,2}$ given in Table 2, n denotes the normal to the wall while y is the distance from the wall (always measured positive into the flow). The role of the function $f(\ell/y)$ is to diminish the magnitude of the wall pressure correction to the total pressure-strain with increased distance from the wall. The form of the f function depends on the length scale ℓ of the energy-containing eddies and for straight channel flows is given by [34]:

$$f\left(\frac{\ell}{y}\right) = f = \frac{k^{3/2}}{C_w \epsilon} \left[\frac{1}{y} + \frac{1}{D-y} \right] \quad (24)$$

where D is the channel width. Eq. (24) reflects the fact that distance-weighted contributions to f at any point in the flow arise from both walls. In the expression the constant C_w is chosen such that $f \rightarrow 1$ as $y \rightarrow 0$. Therefore, setting $\epsilon = C_{\mu}^{3/4} k^{3/2} / \nu y$ (the inertial sub-layer value), in Eq. (24) yields $C_w = \nu / C_{\mu}^{3/4}$.

For straight channel flows the function f is symmetrical with respect to the symmetry plane, where it possesses a minimum value. This is consistent with

Term	Approximation*	Source and Comments
$\Pi_{ij,1}$	$-C_1 \frac{\epsilon}{k} [\overline{u_i u_j} - \frac{2}{3} \delta_{ij} k] ; C_1 = 2.2$	Rotta [36]; Contribution to Π_{ij} from fluctuating velocities only. Return to isotropy proportional to level of anisotropy. Term acts to isotropize $\overline{u_i u_j}$.
$\Pi_{ij,2}$	$-C_2 [P_{ij} - \frac{2}{3} P \delta_{ij}] ; C_2 = 0.55$	Launder, Reece and Rodi [34]; Contribution to Π_{ij} from interaction between mean strain and fluctuating velocities. Term acts to isotropize P_{ij} . P is the production of kinetic energy of turbulence (k): $P = - \frac{\rho}{2} \overline{u_i u_j} \left\{ \frac{\partial U_i}{\partial x_j} + \frac{\partial U_j}{\partial x_i} \right\} ; \text{ see Eq. (11)}$
$\Pi'_{ij,1}$	$C'_1 \frac{\epsilon}{k} (\overline{u_n^2} \delta_{ij} - \frac{3}{2} \overline{u_n u_i} \delta_{nj} - \frac{3}{2} \overline{u_n u_j} \delta_{ni}) f\left(\frac{\ell}{y}\right); C'_1 = 0.75$	Daly and Harlow [35] and Shir [37]; Additive correction to $\Pi_{ij,1}$ due to wall effects. Subscript n denotes direction normal to the wall.
$\Pi'_{ij,2}$	$C'_2 (\Pi_{nm,2} \delta_{ij} - \frac{3}{2} \Pi_{ni,2} \delta_{nj} - \frac{3}{2} \Pi_{nj,2} \delta_{ni}) f\left(\frac{\ell}{y}\right); C'_2 = 0.45$	Gibson and Launder [38]; Additive correction to $\Pi_{ij,2}$ due to wall effects. Subscript n denotes direction normal to the wall.

* Values for C_1, C_2, C'_1 and C'_2 were taken from [29].

TABLE 2: Approximations Used in Pressure-Strain Correlation

the notion that at the symmetry plane the walls of a straight channel should generate equivalent pressure-fluctuation contributions to the pressure-strain terms. The same will not be the case for channel flows in which an asymmetric geometrical condition exists; for example, straight channel flows with one smooth wall and one rough wall, and curved channel flows. In these cases the position of the minimum value of f in the flow will be shifted towards the wall contributing least to changes in the turbulence by wall pressure fluctuation effects; (i.e., the convex wall in a curved channel or the smooth wall in an asymmetrically roughened channel). In this work the location for the minimum in the f function has been assumed to coincide with the location of zero turbulent shear stress. This is consistent with the notion that the length scale of the energy-containing motion, which also transmits the pressure-fluctuations effects, should be smallest at the zero shear stress position. See, for example, the data in [8] and Eq. (30) and related discussion in [2]. In this way the flow is divided into two regions in either one of which the wall nearest to that region is the major source of wall-induced contributions to the pressure-strain correlation.

A general expression for f which accommodates both the symmetric and asymmetric conditions referred to above is:

$$f = \frac{k^{3/2}}{C_w \epsilon} \left[\frac{1}{y} + \frac{(y/D)^m}{D-y} \right] \quad (25)$$

In Eq. (25) y is taken as the distance into the flow measured from the wall which induces the largest contributions to the wall-correction terms: i.e., the rougher of two walls in a straight channel or the concave wall in a curved channel. The value of m can be determined exactly from experimental measurement. For curved channel flows Ellis and Joubert [9] provide the locations of zero turbulent shear stress as a function of curvature ratio. The data can be grouped into strongly curved ($R_c/D < 20$) and mildly curved ($R_c/D > 20$) flows for which the positions of zero shear stress are $y/D = 0.68$ and $y/D = 0.55$ respectively. Setting to zero the y -differentiated general expression for f and using the above values for y yields $m = 7.95$ for strongly curved flows and $m = 2.56$ for mildly curved flows. For $m = 0$ Eq. (25) reduces to the straight channel result given by Eq. (24).

Derivation of the C_μ Function

Following Rodi [28], algebraic expressions for the Reynolds stresses are obtained from Eq. (20) by assuming that the ratio $\overline{u_i u_j}/k$ is constant throughout the flow field. Although inexact, this assumption allows convection minus diffusion of the Reynolds stresses to be expressed as a function of turbulent kinetic energy production (P) and its rate of dissipation (ϵ):

$$U_\ell \frac{\partial \overline{u_i u_j}}{\partial x_\ell} - D_{ij} = \frac{\overline{u_i u_j}}{k} [P - \epsilon] \quad (26)$$

Substitution of Eq. (26) into Eq. (20) yields:

$$\frac{\overline{u_i u_j}}{k} [P - \epsilon] = P_{ij} - \epsilon_{ij} + \Pi_{ij} \quad (27)$$

from which the algebraic relations for $\overline{u_i u_j}$ may be obtained. For the two-dimensional curved channel flow of interest to this work the turbulent stresses $\overline{u_\theta^2}$, $\overline{u_r^2}$ and $\overline{u_\theta u_r}$ are given in cylindrical coordinates in the appendix.

Although the algebraic manipulations are lengthy the general form of C_μ (derived in the appendix) is obtained by substituting Eq. (A-12) for $\overline{u_\theta u_r}$ and Eq. (1) for μ_t into the Boussinesq approximation for $\overline{u_\theta u_r}$:

$$-\overline{u_\theta u_r} = \frac{\mu_t}{\rho} \left(\frac{\partial U_\theta}{\partial r} - \frac{U_\theta}{r} + \frac{1}{r} \frac{\partial U_r}{\partial \theta} \right) \quad (28)$$

The final result may be cast into compact notation form and is given by:

$$C_\mu^{3/2} + a_1 C_\mu + a_2 C_\mu^{1/2} + a_3 = 0 \quad (29)$$

The coefficients in Eq. (29) are also given in the appendix. They are complicated algebraic expressions which may be written in terms of dimensionless velocity gradients (one of which, δ , reflects streamline curvature effects), the ratio P/ϵ , and the wall function f (reflecting the influence of wall pressure fluctuations).

Eq. (29) has only one positive root for $C_\mu^{1/2}$ given by:

$$C_\mu^{1/2} = 2 Q^{1/2} \cos \left[\frac{1}{3} \cos^{-1} (R Q^{-2/3}) \right] - \frac{a_1}{3} \quad (30)$$

with

$$Q = \frac{a_1^2 - 3 a_2}{9}; \quad R = \frac{9 a_1 a_2 - 27 a_3 - 2 a_1^3}{54} \quad (31)$$

Limiting Expressions for the C_μ Function

The general expression for C_μ given by Eq. (30) has several interesting limiting forms attesting to its validity. These are listed below.

Variation of C_μ for flow in the presence of a flat wall. In this case, previously studied by Ljuboja and Rodi [29] in relation to wall jet flows, the influence of pressure-strain (including wall-dampening of velocity fluctuations normal to the wall) is retained in determining the variation of C_μ , but the authors neglect the convective/diffusive transport of $\overline{u_\theta u_r}$ ($u\overline{v}$) in [29]). Also neglected were longitudinal gradients of velocity, and $\frac{\partial U_r}{\partial r} / \frac{\partial U_\theta}{\partial r} \left(\frac{\partial \overline{v}}{\partial y} / \frac{\partial U}{\partial y} \right)$ in [29] was set equal to zero. The latter assumptions correspond here to setting $\delta_a = \delta_b = \delta_c = 0$ in the expressions for a_1 , a_2 and a_3 in C_μ . Also, neglecting the transport of $\overline{u_\theta u_r}$ and realizing that for a flat wall $\delta = 0$, Eq. (30) reduces to:

$$C_\mu = \frac{2}{3} \frac{(1 - C_2) (C_1 - 1 + C_2 P/\epsilon)}{C_1 (C_1 - 1 + P/\epsilon)} \frac{(1 + \frac{3}{2} \frac{C_2 C_2'}{1 - C_2} f)}{(1 + \frac{3}{2} \frac{C_1'}{C_1} f)} \quad (32)$$

$$\times \frac{(1 - 2 \frac{C_2 C_2' P/\epsilon}{C_1 - 1 + C_2 P/\epsilon} f)}{(1 + 2 \frac{C_1'}{C_1 - 1 + P/\epsilon} f)}$$

This is exactly the expression for C_μ obtained in [29]. THE NUMERICAL SCHEME

Variation of C_μ for flow with variable P/ϵ . This case has been investigated by Rodi [28]. Streamline curvature and wall effects in the pressure-strain terms were ignored, but the transport of $\overline{u_\theta u_r}$ ($\overline{u_i u_j}$ in [28]) and variations in the value of P/ϵ were retained in the formulation. The assumptions correspond to setting $\delta_a = \delta_b = \delta_c = \delta = f = 0$ for which Eq. (30) yields:

$$C_\mu = \frac{2}{3} \frac{(1 - C_2)}{C_1} \frac{(1 - (1 - C_2 P/\epsilon)/C_1)}{(1 - (1 - P/\epsilon)/C_1)^2} \quad (33)$$

Eq. (33) corresponds to the expression for C_μ given in [28].

Variation of C_μ for flow with streamline curvature. This case has been studied by Leschziner and Rodi [30] in relation to free jet flow in which local-equilibrium of turbulence was assumed. Wall pressure-corrections and longitudinal gradients of velocity were set equal to zero as was the ratio $\frac{\partial u_r}{\partial r} / \frac{\partial u_\theta}{\partial r}$.

As above, these assumptions lead to setting $\delta_a = \delta_b = \delta_c = f = 0$, in addition to $P = \epsilon$, for which Eq. (30) yields (after lengthy algebraic manipulation):

$$C_\mu = \frac{\frac{2}{3} \left(\frac{1 - C_2}{C_1} \right) \left(\frac{C_2 + C_1 - 1}{C_1} \right)}{1 + 8 \frac{U_\theta}{r} \left(\frac{\partial U_\theta}{\partial r} + \frac{U_\theta}{r} \right) \left(\frac{1 - C_2}{C_1} \right)^2 \left(\frac{k}{\epsilon} \right)^2} \quad (34)^*$$

corresponding to the expression for C_μ given in [30].

Variation of C_μ for flow with small δ in the presence of a curved wall. This case corresponds to the near wall regions of curved channel flow where the local-equilibrium assumption ($P = \epsilon$) applies. Wall-pressure-corrections in the pressure-strain terms are retained by setting $f = 1$, but streamwise gradients of velocity components and $\frac{\partial u_r}{\partial r} / \frac{\partial u_\theta}{\partial r}$ are neglected ($\delta_a = \delta_b = \delta_c = 0$). Taking the limit of Eq. (30) for small δ yields the expression:

$$C_\mu = 0.056 [1 - 12.17 \delta + 0 (\delta^2)] \quad (35)$$

Comparing the above expression with Eq. (2) and recalling Eq. (3) shows that $C_{\mu 0} = 0.056$ and $\beta = 12.17$. This value for β is in good agreement with the values recommended in the literature; for example, Eide and Johnston [39] suggest $\beta = 12$ for both concave and convex walls while Bradshaw [17] recommends $\beta = 9$ at a concave wall and $\beta = 14$ at a convex wall. Similarly, the value for C_μ obtained here falls in the range of values calculated for turbulent wall jets in [29]; in that study the authors found that $C_\mu \approx 0.05$ in the near wall region of their jet flow.

* In the preprint seen by us of reference [30] the 2/3 factor is missing in Eq. (34).

It is required to solve the transport equations (4-6, 9 and 10) in conjunction with the boundary conditions discussed above and summarized in Table 1. Finite difference equations are obtained by volume integration of the transport equations over control volumes or "cells" into which the flow domain is discretized. Details concerning the method for deriving the difference equations and the inclusion of boundary conditions are provided in, for example, [31,41], while an exposition and thorough discussion of the philosophy underlying the calculation approach followed here is available in [42].

The velocity components, pressure, kinetic energy of turbulence and dissipation of kinetic energy of turbulence are the dependent variables calculated on staggered, interconnected grids, each of which is associated with a specific variable (all scalar quantities share the same grid node locations). The general form of the finite difference expressions is given by:

$$\phi_P = \frac{\sum A_i \phi_i + S_o}{\sum A_i + S_P} \quad (36)$$

where ϕ_P represents any one of the dependent variables solved for at the grid node 'P'. The A_i coefficients are determined at the respective cell surfaces and they represent combined contributions arising from diffusion and convection to the balance of ϕ . The terms S_o and S_P represent other contributions arising from sources (or sinks) in the flow [40].

The numerical procedure used to solve the finite difference equations was the Imperial College "TEACH-2E" code [43]. Together with appropriately differenced boundary conditions, elliptic forms* of the equations are solved by means of a cyclic series of predictor-corrector operations involving the use of the tri-diagonal matrix algorithm applied on a line-by-line basis to the calculation domain. From an initial or intermediate value of the pressure field an intermediate velocity field is found. By means of the SIMPLE [42] algorithm, pressure corrections are determined by bringing the intermediate velocity field into conformity with continuity. After corrections to the pressure and velocity fields are applied, the transport equations for kinetic energy of turbulence and its rate of dissipation are solved. Within each iteration various sweeps are made of the entire calculation domain along the main flow direction. The above steps are repeated until a pre-established convergence criterion is satisfied; usually, that the largest of the normalized residuals be less than $5 \cdot 10^{-3}$.

All the numerical calculations were performed on a 20×40 grid, evenly spaced in the main flow (θ) direction and unevenly spaced in the radial (r) direction, after ascertaining that this degree of refinement was sufficiently accurate for the purposes of this study. The storage required on a CDC 7600 computer was 61 k₈ words, and a typical (converged) run time for 300 iterations (3 sweeps per variable) was 130-150 CPU seconds.

* In principle, for the flows calculated here, parabolic equations should suffice since there are no streamwise-reversed flow regions. However, parabolic procedures have been shown [44] to lead to poor estimates of the pressure fields in strongly curved duct flows and dictated the choice of the elliptic scheme.

CALCULATED RESULTS AND DISCUSSION

In this section results are reported of two-dimensional numerical calculations performed using the modified two-equation (k-ε) turbulence model and the general expression for C_μ given by Eq. (30). In the figures this case is referred to as the "extended" k-ε model. The calculations cover both mildly and strongly curved channel flow geometries and include the straight channel flow data of Laufer [45] as a limiting test case. Prior to presenting the calculated cases, however, a discussion is in order regarding the dependence of C_μ on curvature and wall pressure-fluctuation effects. Also, since it is assumed in the derivation of the general expression for C_μ that the ratio $\overline{u_i u_j}/k$ remains constant in the flow, the limitations of this assumption and its effect on the calculations should be assessed.

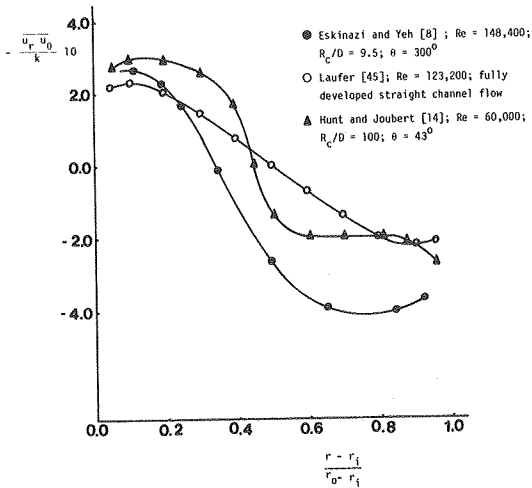


Fig. 1 Transverse variation of $\overline{u_r u_\theta}/k$ (\overline{uv}/k) in fully developed curved and straight channel flows

Figure 1 is a plot of measurements of $\overline{u_\theta u_r}/k$ for three channel flows ranging from strongly curved to straight. In [8] values of k were not provided but could be estimated from the data for $\overline{u_\theta^2}$ and $\overline{u_r^2}$ by assuming that $\overline{u_z^2} \approx \overline{u_\theta^2}$ in $k = \frac{1}{2}(\overline{u_\theta^2} + \overline{u_r^2} + \overline{u_z^2})$. The straight channel flow results show two regions, corresponding to $(r - r_i)/(r_o - r_i) \leq 0.20$ and $(r - r_i)/(r_o - r_i) \geq 0.80$ respectively, wherein $|\overline{u_\theta u_r}/k|$ is approximately constant. Similarly, in the inner-radius wall region the curved channel flows also show relatively constant values of this ratio for $(r - r_i)/(r_o - r_i) \leq 0.20$. By contrast, in the outer-radius wall region, the constancy of the ratio is extended (relative to the straight channel flow case) to values of $(r - r_i)/(r_o - r_i) \geq 0.60$. In the region $0.20 \leq (r - r_i)/(r_o - r_i) \leq 0.65$ the assumption of constant $\overline{u_i u_j}/k$ is obviously invalid and curtails the usefulness of the general expression for C_μ .

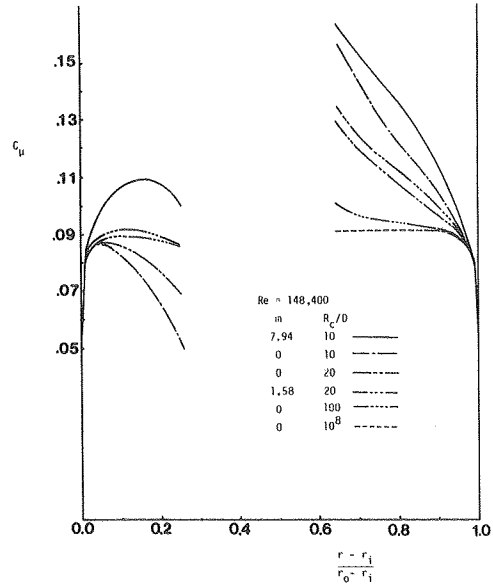


Fig. 2 Transverse variation of C_μ in fully developed curved and straight channel flow. For $m = 0$ wall-function f is symmetric. Calculations based on extended k-ε model.

Figure 2 shows the variation of C_μ as a function of radial position in channels of different curvature. In general C_μ is seen to increase at both walls of a curved channel, at a rate inversely proportional to channel curvature (defined earlier as R_c/D). At the inner-radius wall C_μ reaches a maximum value at a radial location dictated by the channel curvature. As of this location C_μ diminishes with increased distance from the inner-radius wall. For strong curvatures the general function for C_μ yielded unrealistic values of this parameter in the region $0.30 \leq (r - r_i)/(r_o - r_i) \leq 0.65$ due to the lack of constancy in the ratio $\overline{u_i u_j}/k$. However, numerical calculations revealed an insensitivity of the results towards the absolute value of C_μ in this flow region provided that it was contained within the range $0.045 \leq C_\mu \leq 0.140$. This insensitivity is explained, in part, by the small values of $\partial u_\theta/\partial r$ and the respectively counteracting curvature influences which arise in the core region of curved channel flow. In the present study C_μ was set to the value 0.09 in the region $0.30 \leq (r - r_i)/(r_o - r_i) \leq 0.65$.

Wall curvature and wall pressure fluctuations contribute jointly to the value of C_μ . In an effort to separate these two effects, and thereby establish their relative importance, two sets of C_μ profiles in Figure 2 ($R_c/D = 10, 20$) have been calculated with a symmetric distribution of the f function imposed ($m = 0$); equivalent to specifying a straight channel flow condition in so far as wall pressure-corrections

are concerned, while retaining the direct influences of the respective wall curvatures on C_μ . Inspection of these profiles shows that curvature at the outer-radius wall acts to enhance C_μ while curvature at the inner-radius wall acts to suppress it. The inclusion of wall pressure-corrections in the pressure-strain ($m = 1.58$, $m = 7.94$) further increases C_μ at both walls, but at the inner-radius wall the direct influence of curvature effects ultimately overcomes the wall pressure contribution to C_μ causing a net decrease in its value with increasing distance from the inner-radius wall.

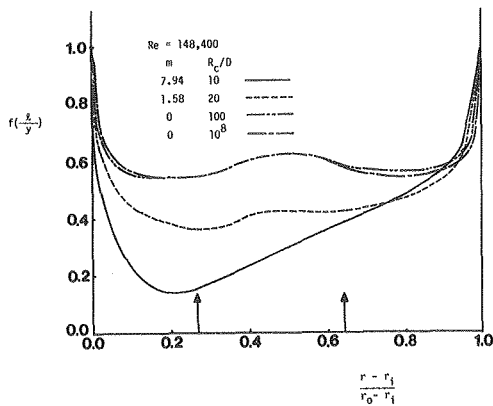


Fig. 3 Transverse variation of wall-function f in fully developed curved and straight channel flow. Arrows denote cut-off values corresponding to C_μ . Calculations based on extended k- ϵ model.

Plots of the f function are shown in Figure 3 for various curvature ratios and, as anticipated, in all cases the function decreases with increased distance from either channel wall, reflecting the decreased influence of wall-corrections to the turbulent flow. The plots also show that at a fixed radial location the f function decreases strongly with increased curvature at the inner-radius wall, while increasing only slightly in the outer-radius wall region bounded by $0.85 \leq (r - r_1)/(r_0 - r_1) \leq 1$. These observations are in agreement with the algebraic stress model predictions in [2] and illustrate the point that convex surfaces are considerably less effective in dampening wall-pressure contributions to turbulent flows than are concave surfaces. Since C_μ can be shown to be inversely proportional to the f wall-function the above observations suggest that pressure fluctuations will contribute more strongly to C_μ at the inner-radius wall than at the outer-radius wall with increasing channel curvature. That this is the case is confirmed by comparing the relative increases between pairs of inner-radius wall C_μ profiles in Figure 2 (with the different f functions specified) for $R_c/D = 20$ and $R_c/D = 10$. By contrast, relative changes in the C_μ

profiles at the outer-radius wall are smaller and of comparable magnitude for both curvatures. This suggests that it is principally the direct influence of curvature effects which determines the shape of the C_μ profiles in the outer-radius flow region, with the magnitude of C_μ being changed only slightly by the wall-pressure effects on the flow. It should be noticed that the same cut-off values set for C_μ apply to the f function since the effects of the latter parameter appear exclusively through the former.

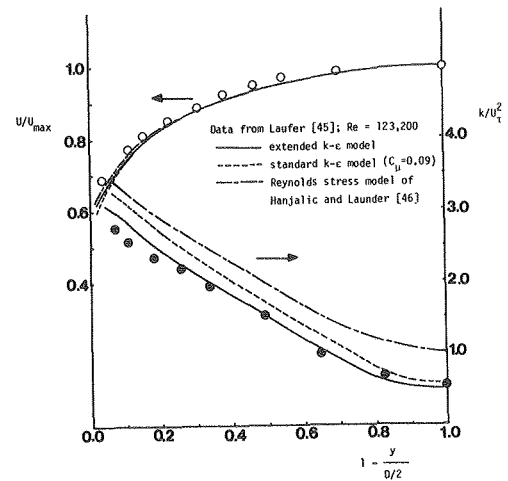


Fig. 4 Transverse variation of normalized streamwise velocity and kinetic energy of turbulence in fully developed straight channel flow. U_{max} and U_τ are maximum and friction velocity respectively.

Prior to conducting curved channel flow predictions, the calculation scheme and the turbulence model in its extended form, including the general formulation for C_μ , were tested by reference to straight channel turbulent flow measurements of Laufer [45]. The law of the wall constants used in Eq. (12) were those specifically recommended by Laufer: $A = 3.0$ and $B = 5.5$. Figure 4 shows predictions using a standard ($C_\mu = 0.09$; $f = 0$) k- ϵ model of turbulence with predictions using the extended version of the model offered here. Also included in the figure are predictions based on the full Reynolds stress closure approach proposed by Hanjalic and Launder [46] (the profiles shown were taken from Hanjalic [47]). While all three models yield excellent agreement between calculated and measured velocity profiles the figure shows that the inclusion of wall pressure-corrections in the general formulation for C_μ leads to an improved prediction of turbulent kinetic energy near the wall. In fact, it is surprising to find that across the whole channel better predictions of k are given by both the two-equation models than by the Reynolds stress closure. Various predictions of flow velocity, friction factor and kinetic energy of turbulence are presented in Figures 5 to 11 for mildly and strongly curved channel flows. Calculations of mean velocity corresponding to the mildly curved ($R_c/D = 100$) channel geometry of Hunt and Joubert [14] provided in Figure 5

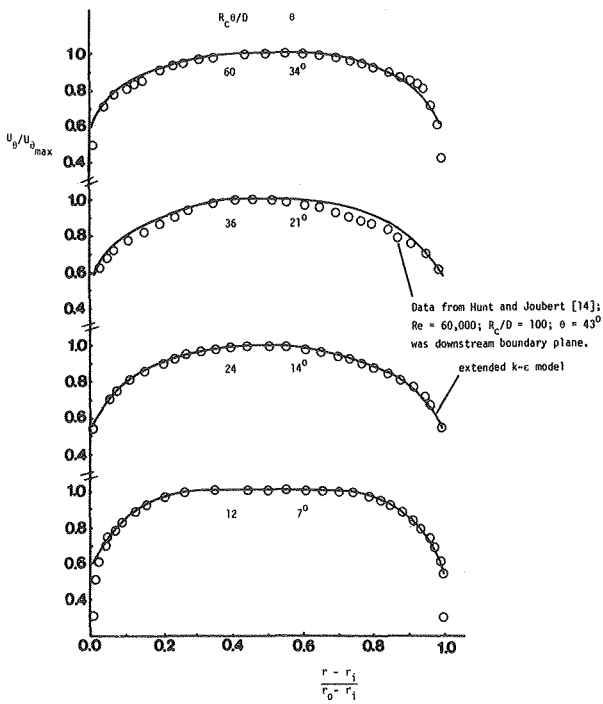


Fig. 5 Transverse variation of normalized streamwise velocity in developing mildly curved channel flow.

show very good agreement with the measurements. Minor deviations are displayed between the measurements and the calculations at $R_c \theta/D = 36$ and 60 in the inner and outer-radius wall regions. These are attributed to the presence of a weak Taylor-Görtler type secondary motion which was observed in the measurements.

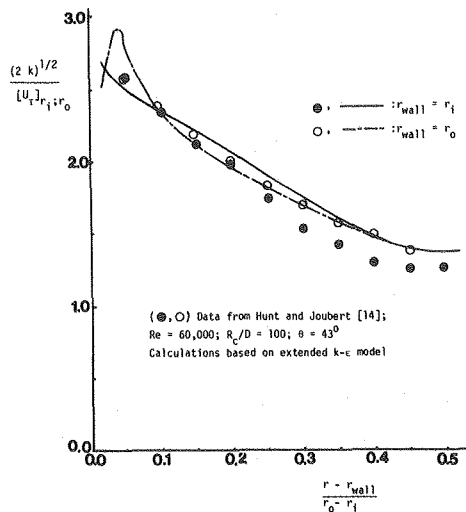


Fig. 6 Transverse variation of kinetic energy of turbulence normalized by respective wall friction velocities in (developed) mildly curved channel flow.

Figure 6 shows good agreement between calculated and measured values of the turbulent kinetic energy in the outer-wall region of the flow. The model overpredicts the measured levels of k by about 17% in the region $0.25 \leq (r - r_i)/(r_o - r_i) \leq 0.50$. This suggests that stabilizing curvature effects on the flow at the convex wall may have been underestimated by the model in this region of the flow.

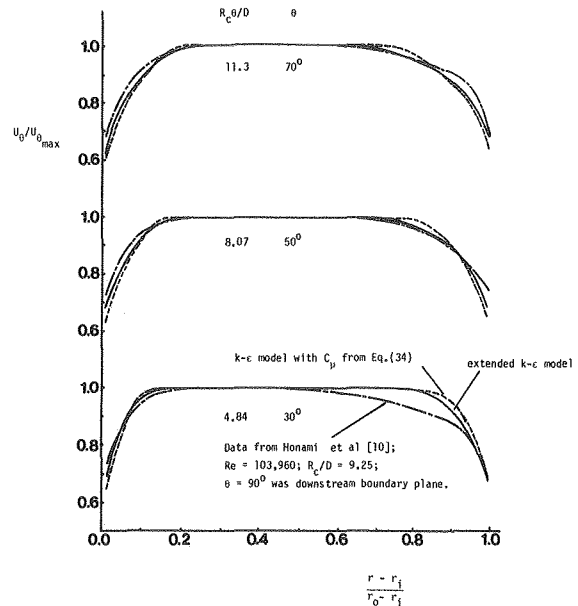


Fig. 7 Transverse variation of normalized streamwise velocity in developing strongly curved channel flow: $Re = 103,960$; $R_c/D = 9.25$.

Calculations for the strongly curved channel geometries of Honami et al [10] ($R_c/D = 9.25$) and Eskinazi and Yeh [8] ($R_c/D = 9.5$) are given in Figures 7 to 10. Mean velocity profiles provided in Figures 7 and 8 show significant discrepancies between measurements and calculations near the outer-radius wall. In both cases the discrepancies are slightly worse when the less general expression for C_μ given by Eq. (34), with only curvature effects retained, is employed. As above, this discrepancy is also attributed to the presence of Taylor-Görtler vortices. The measurements of Honami et al suggest a developing cross-stream motion at the outer-radius wall between $R_c \theta/D = 4.84$ (30°) and $R_c \theta/D = 11.30$ (70°). Similarly, as discussed in the introduction, there is evidence in the shear stress measurements of Eskinazi and Yeh of a Taylor-Görtler type cross-stream flow which would account for part of the discrepancy shown by the results in Figure 8.

Measurements of the friction coefficient from the study of Honami et al are compared in Figure 9 with calculations conducted at three levels of refinement of the $k-\epsilon$ model of turbulence. The best results correspond to the extended $k-\epsilon$ model in which C_μ

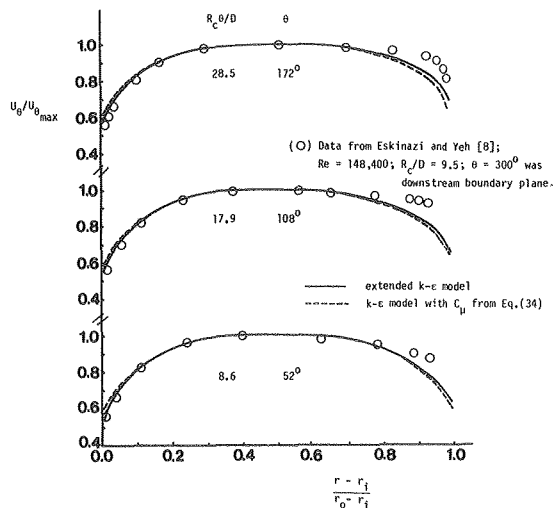


Fig. 8 Transverse variation of normalized streamwise velocity in developing strongly curved channel flow: $Re = 148,400$; $R_c/D = 9.5$.

is specified according to the general Eq. (30) and in which length-scale curvature adjustments are incorporated in the calculation of dissipation and dissipation Prandtl number near the walls. While the agreement between measurements and calculations with the extended model is very good at the inner-radius wall, it is at the outer-wall where inclusion of the above effects produces the largest improvements. The predictions by Honami et al of this flow are also included for comparison. Calculations of the friction coefficient for the flow of Eskinazi and Yeh also yielded similar agreement when using the extended version of the k- ϵ model offered here.

Calculations of the kinetic energy of turbulence for the channel flow of Eskinazi and Yeh are presented in Figure 10. The profiles showing the best overall agreement with the measurements correspond to the present model although differences between models are seen to decrease towards the center of the flow. As for the case of the data of Hunt and Joubert (Figure 6) calculations in the outer-radius wall region are in better agreement with the measurements than at the inner-wall. The magnitude of the discrepancy in the inner-radius wall region appears to be inversely proportional to the curvature ratio (R_c/D) since for the more strongly curved flow of Eskinazi and Yeh the level of k is overpredicted by between 30 to 50%.

Calculations corresponding to the mean velocity measurements of Ellis and Joubert [9] are shown in Figure 11 where they are compared with calculations by Launder et al [7] using a k- ϵ model of turbulence along the lines of Jones and Launder [48]. In the model of Launder et al curvature effects on the length scale of the flow are included via an empirical modification to the dissipation equation. This consists in making the coefficient $C_{\epsilon 2}$ in Eq. (10) a function of a turbulent Richardson number. This approach has been criticized by Gibson [2], and by Rodi [49] who argues that the appropriate place to make such a modification is in the production term of the dissipation equation.

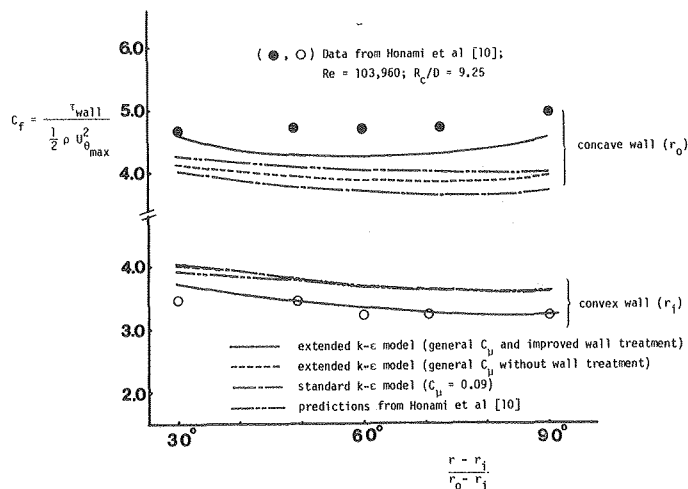


Fig. 9 Streamwise variation of friction factor at the inner and outer walls of strongly curved channel flow.

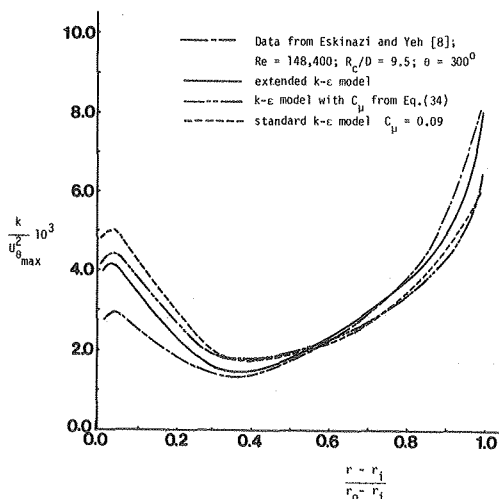


Fig. 10 Transverse variation of normalized kinetic energy of turbulence in strongly curved channel flow.

The predictions of Launder et al show slightly better agreement with the measurements at the outer-radius wall, but at the inner-wall the present model yields better results. It is difficult to decide on the basis of this limited comparison which model is better for the prediction of curved channel flows in general. However, in view of the points raised by Gibson [2] and by Rodi [49], and given the fact that the model of Launder et al requires an additional

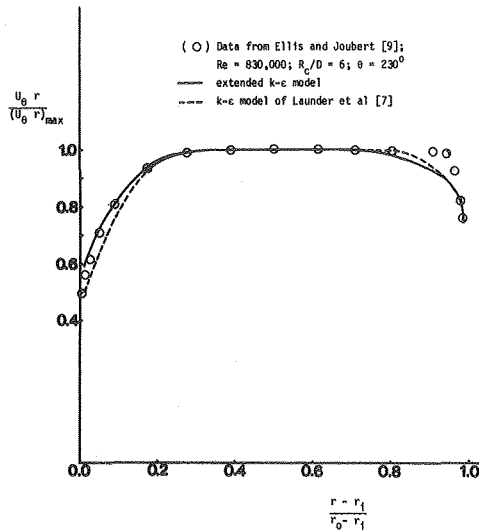


Fig. 11 Transverse variation of normalized angular momentum in strongly curved channel flow.

constant and its numerical optimization, it would seem that the model offered here is of a more general nature.

CONCLUSIONS

By consideration of Reynolds stress equations in algebraically modeled form a general expression has been derived for the coefficient C_μ in the expression for turbulent viscosity $\nu_t = C_\mu k^2/\epsilon$. The generalized form of this coefficient includes streamline curvature and wall pressure fluctuation effects and, hence, their influence on the turbulent length scale ($k^{3/2}/\epsilon$) in the flow. The expression derived has been shown to include limiting forms given by less general formulations obtained in other works. One of these forms corresponds to the proposal by Bradshaw, Eq. (3) in the text, and yields values of the constants $\beta = 12.17$ and $C_{\mu 0} = 0.056$ which are in good agreement with values established in the literature.

Predictions of developing two-dimensional curved channel flow have been conducted by incorporating the general expression for C_μ into a $k-\epsilon$ model of turbulence modified to include the direct influence of curvature effects on the length scale in near-wall regions of the flow. In general, agreement between the measurements and the calculations is good. The largest discrepancies observed in the calculations of mean velocity arise at the outer-radius wall and are attributed to the existence of cross-stream motions (Taylor-Görtler vortices) in the experiments. The present model consistently over-predicts the kinetic energy of turbulence in the inner-radius wall region of curved channel flow. The degree of overprediction is inversely proportional to mean channel curvature (R_c/D). This discrepancy is attributed to a failing of the model to accommodate fully the stabilizing influences of convex curvature on turbulent flow due to the breakdown of the assumption underlying the

formulation, that $\overline{u_i u_j}/k$ is a constant everywhere in the flow.

It is a noteworthy feature of the extended $k-\epsilon$ model presented here that none of the previously established model constants have been modified or fine-tuned to yield improved agreement between predictions and measurements. This includes the new parameter m appearing in the f wall-function which is determined exactly from experimental measurement as opposed to being optimized numerically. In this sense the present model provides a more general formulation than models based on the ad-hoc inclusion of a flux Richardson number (and its associated model constant) in the equation for dissipation of kinetic energy of turbulence.

ACKNOWLEDGEMENTS

Funding for this study was provided by the Division of Material Sciences, Office of Basic Energy Sciences, U.S. Department of Energy under Contract number W-7405-ENG-48. We welcome this opportunity to express our appreciation for this support.

REFERENCES

1. Wilcox, D.C. and Chambers, T.L., "Streamline Curvature Effects on Turbulent Boundary Layers," AIAA Journal, Vol. 15, No. 4, 1977, pp. 574-580.
2. Gibson, M.M., "An Algebraic Stress and Heat-Flux Model for Turbulent Shear Flow with Streamline Curvature," International Journal of Heat and Mass Transfer, Vol. 21, 1978, pp. 1609-1617.
3. Simon, T.W. and Moffat, R.J., "Heat Transfer Through Turbulent Boundary Layers - The Effects of Introduction of and Recovery From Convex Curvature," Paper No. 79-WA/GT-10, Dec., 1979, Presented at the ASME Winter Annual Meeting, New York, N.Y.
4. Tani, I., "Production of Longitudinal Vortices in the Boundary Layer Along a Concave Wall," Journal of Geophysical Research, Vol. 67, No. 8, 1962, pp. 3075-3080.
5. Rotta, J.C., "Effects of Streamwise Wall Curvature on Compressible Turbulent Boundary Layers," The Physics of Fluids Supplement, 1967, S174-S180.
6. Irwin, H.P.A.H. and Smith P. Arnot, "Prediction of the Effect of Streamline Curvature on Turbulence," The Physics of Fluids, Vol. 18, No. 6, 1975, pp. 624-630.
7. Launder, B.E., Priddin, C.H., and Sharma, B.I., "The Calculation of Turbulent Boundary Layers on Spinning and Curved Surfaces," Trans. ASME, Journal of Fluids Engineering, 1977, pp. 231-239.
8. Eskinazi, S., and Yeh, H., "An Investigation on Fully Developed Turbulent Flows in a Curved Channel," Journal of Aeronautical Sciences, 1956, pp. 23-34.
9. Ellis, L.B. and Joubert, P.N., "Turbulent Shear Flow in a Curved Duct," Journal of Fluid Mechanics, Vol. 62, Part 1, 1974, pp. 65-84.
10. Honami, S., Ariga, I., Abe, T. and Watanabe, I., "Investigation of Turbulent Flows in Curved Channels," Paper No. 75-FE-32, May 5-7, 1975, Presented at the ASME Joint Fluids Engineering and Lubrication Conference.

11. Meroney, R.N. and Bradshaw, P., "Turbulent Boundary-Layer Growth Over a Longitudinally Curved Surface," AIAA Journal, Vol. 13, No. 11, 1975, pp. 1446-1453.
12. Blottner, F.G., "Entry Flow in Straight and Curved Channels with Slender Channel Approximations," Trans. ASME, Journal of Fluids Engineering, Vol. 99, 1977, pp. 666-674.
13. Brinich, P.F. and Graham, R.W., "Flow and Heat Transfer in a Curved Channel," NASA TN D-8464, 1977.
14. Hunt, I.A. and Joubert, P.N., "Effects of Small Streamline Curvature on Turbulent Duct Flow," Journal of Fluid Mechanics, Vol. 91, Part 4, 1979, pp. 633-659.
15. So, R.M., "A Turbulence Velocity Scale for Curved Shear Flows," J. Fluid Mechanics, Vol. 70, Part 1, 1975, pp. 37-57.
16. Prabhu, A. and Sundarasiva Rao, B.N., "On the Large-Scale Structure in Turbulent Boundary Layers on Curved Surfaces," Paper presented at the Joint ASME/ASCE Mechanics Conference, University of Colorado, Boulder, Colorado, June 22-24, 1981.
17. Bradshaw, P., "Effects of Streamline Curvature on Turbulent Flow," AGARDograph No. 169, 1973.
18. Kreith, F., "The Influence of Curvature on Heat Transfer to Incompressible Fluids," Trans. ASME, Vol. 77, No. 11, 1955, pp. 1247-1256.
19. Thomann, H., "Effect of Streamwise Wall Curvature Heat Transfer in a Turbulent Boundary Layer," Journal of Fluid Mechanics, Vol. 33, Part 2., 1968, pp. 283-292.
20. Mayle, R.E., Blair, M.F. and Kopper, F.C., "Turbulent Boundary Layer Heat Transfer on Curved Surfaces," Journal of Heat Transfer, Vol. 101, No. 3, 1979, pp. 515-523.
21. Taylor, G.I., "Stability of Viscous Liquid Contained Between Two Rotating Cylinders," Philosophical Transactions of the Royal Society (London), Vol. 223, 1923, pp. 289-343.
22. Taylor, G.I., "Distribution of Velocity and Temperature Between Concentric Rotating Cylinders," Proceedings of the Royal Society of London, Series A, Vol. 151, 1935, pp. 494-512.
23. Görtler, H., "Über Eine Dreidimensionale Instabilität Laminarer Grenz-Schichten an Konkaven Wänden," Nachr. Ges. Wiss. Göttingen, Math.-phys. Kl., Vol. 2(1), 1940. Also available as NACA TM 1375, 1942.
24. Patel, V.C., "Measurements of Secondary Flow in the Boundary Layers of a 180 Degree Channel," Aero. Res. Council Current Paper No. 1043, 1968.
25. Kelleher, M.D., Flentil, D.L. and McKeen, R.J., "An Experimental Study of the Secondary Flow in a Curved Rectangular Channel," Paper No. 79-FE-6, Dec., 1979, Presented at the ASME Winter Annual Meeting, New York, N.Y.
26. Lezius, D.K. and Johnston, J.P., Stanford University, Department of Mechanical Engineering, Thermo-Science Division, Report MD-29, 1971.
27. Simon, T.W. and Honami, S., "Summary of Data Evaluation for Boundary Layer Flows with Streamwise Curvature, Case 0230," The 1980-81 AFOSR-HTTM-Stanford Conference on Complex Turbulent Flows: Comparison of Computation and Experiment, Stanford University, Stanford, California, September 1980.
28. Rodi, W., "A New Algebraic Relation for Calculating the Reynolds Stresses," Mechanics of Fluid, ZAMM, Vol. 56, 1976, pp. T219-T221.
29. Ljuboja, M. and Rodi, W., "Calculation of Turbulent Wall Jets with an Algebraic Reynolds Stress Model," Proceedings of the ASME Symposium on Turbulent Boundary Layers, Niagara Falls, N.Y., June 1979.
30. Leschziner, M.A. and Rodi, W., "Calculation of Annular and Twin Parallel Jets Using Various Discretization Schemes and Turbulence Model Variants," to appear in J. Fluids Eng., Trans. ASME, 1981.
31. Humphrey, J.A.C., Whitelaw, J.H. and Yee, G., "Turbulent Flow in a Square Duct with Strong Curvature," Journal of Fluid Mechanics, Vol. 103, 1981, pp. 443-463.
32. Jones, W.P. and Launder, B.E., "The Prediction of Laminarization With a Two-Equation Model of Turbulence," International Journal of Heat and Mass Transfer, Vol. 15, 1972, pp. 301-314.
33. Launder, B.E. and Spalding, D.B., "The Numerical Computation of Turbulent Flows," Computer Methods in Applied Mechanics and Engineering, Vol. 3, 1974, pp. 269-289.
34. Launder, B.E., Reece, G.J. and Rodi, W., "Progress in the Development of a Reynolds-Stress Turbulence Closure," J. Fluid Mechanics, Vol. 68, Part 3, 1975, pp. 537-566.
35. Daly, B.J. and Harlow, F.H., "Transport Equations of Turbulence," Phys. Fluids, Vol. 13, 1970, p. 2634.
36. Rotta, J.C., "Turbulente Stromungen," B.G. Teubner, Stuttgart, 1972.
37. Shir, C.C., "A Preliminary Numerical Study of Atmospheric Turbulent Flow in the Idealized Planetary Boundary Layer," J. Atmos. Sci., Vol. 30, 1973, p. 1327.
38. Gibson, M.M. and Launder, B.E., "Ground Effects on Pressure Fluctuations in the Atmospheric Boundary," J. Fluid Mechanics, Vol. 86, 1978, p. 491.
39. Eide, S.A. and Johnston, J.P., "Prediction of the Effects of Longitudinal Wall Curvature and System Rotation on Turbulent Boundary Layers," Dept. Mech. Eng., Stanford University, Stanford, CA., 1974, Report No. PD-19.
40. Humphrey, J.A.C., "Numerical Calculation of Developing Laminar Flow in Pipe of Arbitrary Curvature Radius," Can. J. Chem. Eng., Vol. 56, 1978, p. 151.

41. Humphrey, J., Taylor, A., and Whitelaw, J.H., "Laminar Flow in a Square Duct of Strong Curvature," J. Fluid Mechanics, Vol. 83, 1977, pp. 509-527.

42. Patankar, S.V., "Numerical Heat Transfer and Fluid Flow," Hemisphere Publishing Corporations, McGraw-Hill Book Company, 1980.

43. Gosman, A.D. and Pun, W.M., "Lecture Notes for Course Entitled: Calculation of Recirculating Flows," Imperial College Report No. HTS/74/2, 1974, London University.

44. Yee, G., Chilukuri, R., and Humphrey, J.A.C., "Developing Flow and Heat Transfer in Strongly Curved Ducts of Rectangular Cross Section," Journal of Heat Transfer, Trans. AMSE, Vol. 102, 1980, pp. 285-291.

45. Laufer, J., "Investigation of Turbulent Flow in a Two-Dimensional Channel," NACA Technical Note 2123, 1950.

46. Hanjalic, K. and Launder, B.E., "A Reynolds Stress Model of Turbulence and its Application to Thin Shear Flows," J. Fluid Mech., Vol. 52, Part 4, 1972, pp. 609-638.

47. Hanjalic, K., "Two-Dimensional Asymmetric Turbulent Flow in Ducts," Ph.D. Thesis, 1970, University of London.

48. Jones, W.P. and Launder, B.E., "The Prediction of Laminarization with a 2-Equation Model of Turbulence," Int. J. Heat Mass Transfer, Vol. 15, 1972, p. 301.

49. Rodi, W., "Influence of Buoyancy and Rotation on Equations for the Turbulent Length Scale," Proceedings of the 2nd Symposium on Turbulent Shear Flows, July 1979, Imperial College, London University.

50. Pourahmadi, F., "Turbulence Modeling of Single and Two-Phase Curved Channel Flows," Ph.D. Thesis, Department of Mechanical Engineering, University of California, Berkeley campus, to be submitted December 1981.

APPENDIX: DETAILED DERIVATION OF GENERAL C_μ FUNCTION

The starting point for the derivation of the C_μ function is Eq. (20) in the main text. Noting that the diffusion terms D_{ij} are never actually required in the formulation and that $U_z = 0$ and $\frac{\partial}{\partial z} = 0$, (assumption of 2-D mean flow) Eq. (20) yields the following expressions for u_θ^2 , u_r^2 and $\overline{u_\theta u_r}$ in cylindrical coordinates:

$$\begin{aligned} \frac{Du_\theta^2}{Dt} - D_{\theta\theta} &= -2 \frac{u_\theta^2}{r} \frac{\partial U_\theta}{\partial \theta} - 2 \overline{u_\theta u_r} \left(\frac{\partial U_\theta}{\partial r} + \frac{U_\theta}{r} \right) \\ &- 2 \frac{U_r}{r} \overline{u_\theta^2} + 2 \frac{p}{\rho} \frac{\partial u_\theta}{r \partial \theta} - \frac{2}{3} \epsilon \end{aligned} \quad (A-1)$$

$$\begin{aligned} \frac{Du_r^2}{Dt} - D_{rr} &= 4 \overline{u_\theta u_r} \frac{U_\theta}{r} - 2 \overline{u_r^2} \frac{\partial U_r}{\partial r} - 2 \overline{u_\theta u_r} \frac{\partial U_r}{r \partial \theta} \\ &+ 2 \frac{p}{\rho} \frac{\partial u_r}{\partial r} - \frac{2}{3} \epsilon \end{aligned} \quad (A-2)$$

$$\begin{aligned} \frac{Du_\theta u_r}{Dt} - D_{\theta r} &= (2 \overline{u_\theta^2} - \overline{u_r^2}) \frac{U_\theta}{r} - \overline{u_r^2} \frac{\partial U_\theta}{\partial r} \\ &- \frac{u_\theta^2}{r} \frac{\partial U_r}{\partial \theta} + \frac{p}{\rho} \frac{\partial u_\theta}{\partial r} + \frac{p}{\rho} \frac{\partial u_r}{r \partial \theta} \end{aligned} \quad (A-3)$$

where, for convenience, $\frac{D}{Dt} = \frac{\partial}{\partial t} + U_r \frac{\partial}{\partial r} + \frac{U_\theta}{r} \frac{\partial}{\partial \theta}$ has been used even though $\partial/\partial t = 0$. In Eqs. A.1 - A.3 contributions to the pressure-strain terms are modeled according to Eq. (22) and Table 2. In cylindrical coordinates, these terms are:

$$\begin{aligned} 2 \frac{p}{\rho} \frac{\partial u_\theta}{r \partial \theta} &= -C_1 \frac{\epsilon}{k} (\overline{u_\theta^2} - \frac{2}{3} k - \frac{C'_1}{C_1} f \overline{u_r^2}) \\ &- C_2 \left\{ -2 \overline{u_\theta u_r} \left(\frac{\partial U_\theta}{\partial r} + \frac{U_\theta}{r} \right) - 2 \overline{u_\theta^2} \frac{\partial U_\theta}{r \partial \theta} - 2 \frac{U_r}{r} \overline{u_\theta^2} \right. \\ &+ C'_2 f \left[4 \overline{u_\theta u_r} \frac{U_\theta}{r} + 2 \overline{u_r^2} \left(\frac{\partial U_\theta}{r \partial \theta} + \frac{U_r}{r} \right) - 2 \overline{u_\theta u_r} \frac{\partial U_r}{r \partial \theta} \right] \\ &\left. - \frac{2}{3} P (1 + C'_2 f) \right\} \end{aligned} \quad (A-4)$$

$$\begin{aligned} 2 \frac{p}{\rho} \frac{\partial u_r}{\partial r} &= -C_1 \frac{\epsilon}{k} \left[(1 + 2 \frac{C'_1}{C_1} f) \overline{u_r^2} - \frac{2}{3} k \right] \\ &- C_2 (1 - 2 C'_2 f) \left[\overline{u_\theta u_r} \left(4 \frac{U_\theta}{r} - 2 \frac{\partial U_r}{r \partial \theta} \right) \right. \\ &\left. + 2 \overline{u_r^2} \left(\frac{\partial U_\theta}{r \partial \theta} + \frac{U_r}{r} \right) - \frac{2}{3} P \right] \end{aligned} \quad (A-5)$$

$$\begin{aligned} \frac{p}{\rho} \left(\frac{1}{r} \frac{\partial \overline{u_\theta u_r}}{\partial \theta} + \frac{\partial \overline{u_\theta u_r}}{\partial r} \right) &= -C_1 \frac{\epsilon}{k} \overline{u_\theta u_r} \left(1 + \frac{3}{2} \frac{C'_1}{C_1} f \right) \\ &+ C_2 (1 - \frac{3}{2} C'_2 f) \left[\overline{u_r^2} \frac{\partial U_\theta}{\partial r} - (2 \overline{u_\theta^2} - \overline{u_r^2}) \frac{U_\theta}{r} + \overline{u_\theta^2} \frac{\partial U_r}{r \partial \theta} \right] \end{aligned} \quad (A-6)$$

From Eq. (26) in the main text:

$$\frac{D u_\theta^2}{Dt} - D_{\theta\theta} = \frac{\overline{u_\theta^2}}{k} (P - \epsilon) \quad (A-7)$$

$$\frac{D u_r^2}{Dt} - D_{rr} = \frac{\overline{u_r^2}}{k} (P - \epsilon) \quad (A-8)$$

$$\frac{D}{Dt} \overline{u_\theta u_r} - D_{\theta r} = \frac{\overline{u_\theta u_r}}{k} (P - \epsilon) \quad (A-9)$$

Eqs. A-1 to A-9 lead to a system of algebraic equations which can be solved for the three unknowns $\overline{u_\theta^2}$, $\overline{u_r^2}$ and $\overline{u_\theta u_r}$. The result is:

$$\overline{u_\theta^2} = \frac{d(nl - jg) - n(bl - cj) + m(bg - cn)}{a(nl - gj) - e(bl - cj) + i(bg - cn)} \quad (A-10)$$

$$\overline{u_r^2} = \frac{a(hl - mg) - e(dl - mc) + i(dg - hc)}{a(nl - gj) - e(bl - cj) + i(bg - cn)} \quad (A-11)$$

$$\overline{u_\theta u_r} = \frac{a(nm - hj) - e(bm - dj) + i(bh - dn)}{a(nl - gj) - e(bl - cj) + i(bg - cn)} \quad (A-12)$$

with the following values for the coefficients in the above expressions:

$$a = 0 \quad (A-13)$$

$$b = \frac{1}{k} [P - (1 - C_1 + 2C_1' f) \epsilon] + 2(1 - C_2 + 2C_2' f) \frac{\partial U_r}{\partial r} \quad (A-14)$$

$$c = 2(C_2 - 2C_2' C_2' f - 1) \left(2 \frac{U_\theta}{r} - \frac{\partial U_r}{r \partial \theta} \right) \quad (A-15)$$

$$d = \frac{2}{3} \epsilon [C_1 - 1 + C_2(1 - 2C_2' f) \frac{P}{\epsilon}] \left(2 \frac{U_\theta}{r} - \frac{1}{r} \frac{\partial U_r}{\partial \theta} \right) \quad (A-16)$$

$$e = [1 - C_2(1 - \frac{3}{2} C_2' f)] \left(2 \frac{U_\theta}{r} - \frac{1}{r} \frac{\partial U_r}{\partial \theta} \right) \quad (A-17)$$

$$n = -[1 - C_2(1 - \frac{3}{2} C_2' f)] \left(\frac{\partial U_\theta}{\partial r} + \frac{U_\theta}{r} \right) \quad (A-18)$$

$$g = -\frac{1}{k} [P - (1 - C_1 - \frac{3}{2} C_1' f) \epsilon] \quad (A-19)$$

$$h = 0 \quad (A-20)$$

$$i = \frac{1}{k} [P + (C_1 - 1) \epsilon] - 2(1 - C_2) \frac{\partial U_r}{\partial r} \quad (A-21)$$

$$j = -C_1' f \frac{\epsilon}{k} - 2C_2' C_2' f \frac{\partial U_r}{\partial r} \quad (A-22)$$

$$l = 2(1 - C_2) \frac{\partial U_\theta}{\partial r} + \frac{U_\theta}{r} + C_2' C_2' f \left(4 \frac{U_\theta}{r} - \frac{2}{r} \frac{\partial U_r}{\partial \theta} \right) \quad (A-23)$$

$$m = \frac{2}{3} [(C_1 - 1) \epsilon + C_2(1 + C_2' f) P] \quad (A-24)$$

Combining the Boussinesq approximation for $\overline{u_\theta u_r}$, as given by Eq. (28) in the main text, with the algebraically derived expression for $\overline{u_\theta u_r}$ given above yields a general expression for C_μ of the form:

$$C_\mu = \frac{\alpha_1 + \beta_1 \frac{k}{\epsilon} \frac{\partial U_\theta}{\partial r}}{(1 - \delta + \delta_c) \left[\alpha_2 + \beta_2 \left(\frac{k}{\epsilon} \frac{\partial U_\theta}{\partial r} \right) + \gamma_2 \left(\frac{k}{\epsilon} \frac{\partial U_\theta}{\partial r} \right)^2 + \delta_2 \left(\frac{k}{\epsilon} \frac{\partial U_\theta}{\partial r} \right)^3 \right]} \quad (A-25)$$

where α_1 , β_1 , α_2 , β_2 , γ_2 and δ_2 are lengthy algebraic functions of the flow variables and turbulence constants*.

Eq. (A-25) does not show the explicit dependence of

C_μ on the parameters, $\delta_a = \frac{\partial U_\theta / \partial U_\theta}{r \partial \theta / \partial r}$, $\delta_b = \frac{\partial U_r / \partial U_\theta}{\partial r / \partial r}$,

$\delta_c = \frac{\partial U_\theta / \partial U_\theta}{r \partial \theta / \partial r}$, $\delta = \frac{U_\theta / \partial U_\theta}{r / \partial r}$, the wall-function f and the ratio P/ϵ . Using Eq. (11) in the main text it is possible to show that:

$$\frac{k}{\epsilon} \frac{\partial U_\theta}{\partial r} = \frac{\pm (P/\epsilon)^{1/2}}{C_\mu^{1/2} [(1 - \delta + \delta_c)^2 + 4 \delta_b^2]^{1/2}} \quad (A-26)$$

with a positive sign preceding the above expression when

$\frac{\partial U_\theta}{\partial r} > 0$ and negative when $\frac{\partial U_\theta}{\partial r} < 0$. Substitution of

Eq. (A-26) into Eq. (A-25) yields (after algebraic manipulation):

$$C_\mu^{3/2} + a_1 C_\mu + a_2 C_\mu^{1/2} + a_3 = 0 \quad (A-27)$$

with:

$$a_1 = \pm \frac{2[(D + P/\epsilon)(1 - B) - F(A - 1 + P/\epsilon)] \delta_b (P/\epsilon)^{1/2}}{(D + P/\epsilon)(A - 1 + P/\epsilon)[1 - \delta + \delta_c]^2 + 4 \delta_b^2]^{1/2}} \quad (A-28)$$

* Expressions for these functions are available in Pourahmadi [50].

$$\begin{aligned}
a_2 = & \left\{ -E(2\delta - \delta_c) \left\{ (A - 1 + P/\epsilon) [2F(1 + \delta) + 2C_2 C_2' f(2\delta - \delta_c)] + 2C_1' f(1 - B)(\delta_c - 2\delta) \right\} \right. \\
& + 2E(D + P/\epsilon)(1 - B)(\delta_c - 2\delta)(1 + \delta) + 4F(1 - C_2) \delta_b^2 (1 - B)(G - 1 + P/\epsilon) \left. \right\} \\
& \times P/\epsilon \left/ \left\{ [(1 - \delta + \delta_c)^2 + 4\delta_b^2] [-(D + P/\epsilon)(A - 1 + P/\epsilon)(G - 1 + P/\epsilon)] \right\} \right. \\
& + \left\{ -E(2\delta - \delta_c) \left\{ 2/3(D + 1 + P/\epsilon)(A - 1 + P/\epsilon) + 2/3(D + B P/\epsilon) C_1' f \right\} \right. \\
& \left. + E(1 + \delta) [2/3(D + B P/\epsilon)](D + P/\epsilon) \right\} \left/ \left\{ -(D + P/\epsilon)(A - 1 + P/\epsilon)(G - 1 + P/\epsilon)(1 - \delta + \delta_c) \right\} \right.
\end{aligned} \tag{A-29}$$

$$\begin{aligned}
a_3 = & \mp \left\{ E(2\delta - \delta_c) \delta_b \left\{ 2(1 - B) [2F(1 + \delta) + 2C_2 C_2' f(2\delta - \delta_c)] + 4(1 - B)(\delta_c - 2\delta) C_2 C_2' f \right\} \right. \\
& + 4EF(1 - B)(\delta_c - 2\delta)(1 + \delta) \delta_b \left. \right\} \left[\frac{P/\epsilon}{[(1 - \delta + \delta_c)^2 + 4\delta_b^2]} \right]^{3/2} \left/ \left\{ -(D + P/\epsilon)(A - 1 + P/\epsilon)(G - 1 + P/\epsilon) \right\} \right. \\
& \mp \left\{ 2/3 E(2\delta - \delta_c) \delta_b \left\{ 2(D + H P/\epsilon)(1 - B) + 2(D + B P/\epsilon) C_2 C_2' f \right\} \right. \\
& + 4/3 E(1 + \delta)(D + B P/\epsilon) F \delta_b \left. \right\} \left[\frac{P/\epsilon}{[(1 - \delta + \delta_c)^2 + 4\delta_b^2]} \right]^{1/2} \\
& \left/ \left\{ -(D + P/\epsilon)(A - 1 + P/\epsilon)(G - 1 + P/\epsilon)(1 - \delta + \delta_c) \right\} \right.
\end{aligned} \tag{A-30}$$

In the above expressions:

$$\begin{aligned}
A &= C_1 (1 + 2f C_1'/C_1) \\
B &= C_2 (1 - 2f C_2') \\
D &= C_1 - 1 \\
E &= 1 - C_2 (1 - 3/2 f C_2') \\
F &= 1 - C_2 \\
G &= C_1 (1 + 3/2 f C_1'/C_1) \\
H &= C_2 (1 + f C_2')
\end{aligned} \tag{A-31}$$